Acta Pharmaceutica Sinica B 2023;13(1):359−371

Chinese Pharmaceutical Association
Institute of Materia Medica, Chinese Academy of Medical Sciences

Acta Pharmaceutica Sinica B

www.elsevier.com/locate/apsb
www.sciencedirect.com

ORIGINAL ARTICLE

All-stage targeted therapy for the brain metastasis from triple-negative breast cancer

Zimiao Luo[a,d], Sunyi Wu[a,d], Jianfen Zhou[a,d], Weixia Xu[a,d], Qianzhu Xu[a,b,d], Linwei Lu[b], Cao Xie[a,d], Yu Liu[a,d], Weiyue Lu[a,b,c,d,*]

[a]*Department of Pharmaceutics, School of Pharmacy, Key Laboratory of Smart Drug Delivery, Fudan University, Shanghai 201203, China*
[b]*Department of Integrative Medicine, Huashan Hospital, Institutes of Integrative Medicine of Fudan University, Shanghai 200041, China*
[c]*Minhang Branch, Zhongshan Hospital and Institute of Fudan-Minghang Academic Health System, Minghang Hospital, Fudan University, Shanghai 201199, China*
[d]*State Key Laboratory of Medical Neurobiology, Collaborative Innovation Center for Brain Science, Fudan University, Shanghai 200032, China*

Received 21 February 2022; received in revised form 28 March 2022; accepted 30 March 2022

KEY WORDS

Breast cancer;
Brain metastasis from breast cancer;
Platelet-hybrid liposome;
pVAP peptide;
Nanocrystal;
Cabazitaxel;
Targeted drug delivery;
Drug delivery system

Abstract Brain metastasis is a common and serious complication of breast cancer, which is commonly associated with poor survival and prognosis. In particular, the treatment of brain metastasis from triple-negative breast cancer (BM-TNBC) has to face the distinct therapeutic challenges from tumor heterogeneity, circulating tumor cells (CTCs), blood−brain barrier (BBB) and blood−tumor barrier (BTB), which is in unmet clinical needs. Herein, combining with the advantages of synthetic and natural targeting moieties, we develop a "Y-shaped" peptide pVAP-decorated platelet-hybrid liposome drug delivery system to address the all-stage targeted drug delivery for the whole progression of BM-TNBC. Inherited from the activated platelet, the hybrid liposomes still retain the native affinity toward CTCs. Further, the peptide-mediated targeting to breast cancer cells and transport across BBB/BTB are demonstrated *in vitro* and *in vivo*. The resultant delivery platform significantly improves the drug accumulation both in orthotopic breast tumors and brain metastatic lesions, and eventually exhibits an outperformance in the inhibition of BM-TNBC compared with the free drug. Overall, this work provides a promising prospect for the comprehensive treatment of BM-TNBC, which could be generalized to other cell types or used in imaging platforms in the future.

*Corresponding author.
E-mail address: wylu@shmu.edu.cn (Weiyue Lu).

Peer review under responsibility of Chinese Pharmaceutical Association and Institute of Materia Medica, Chinese Academy of Medical Sciences.

https://doi.org/10.1016/j.apsb.2022.03.026

1. Introduction

Cancer metastasis to brain remains a fatal clinical reality in most cases, resulting an estimated survival time of several months in spite of palliative treatments[1]. Among all breast cancer subtypes, triple-negative breast cancer (TNBC) has the highest incidence of brain metastasis and the poorest prognosis[2]. Women with brain metastasis from TNBC suffer the most intractable therapeutic challenges concurrently from the tumor heterogeneity, circulating tumor cells (CTCs), blood−brain barrier (BBB) and blood−tumor barrier (BTB)[3−6]. Ideal treatment strategies for brain metastatic TNBC with an all-stage cure of *in situ* tumors, CTCs and metastatic lesions are in unmet medical needs.

Liposomes is one of the most mature and widely used nanoscale delivery platform. Over the past several years, natural human, murine or bacterial cell membrane materials were partly or totally incorporated into liposomes in virtue of their unique physiological functions[7−9]. For example, activated platelet membranes were employed to target solid tumors, CTCs or metastatic lesions[10−13]. While the scarce membrane sources, complex extraction steps and compromised circulation half-lives limited the translation of platelet vehicle systems into clinical applications[14]. Inspired by this, we hypothesize that a membrane-hybrid liposome delivery platform with a proper proportion of platelet membranes and lipids might provide a desirable solution to balance the targeting and long systemic circulation.

The off-targeting and BBB-derived rigid obstacle of drug delivery into the brain are considered another two challenges during the treatment of brain metastatic TNBC. Glucose-regulated protein 78 (GRP78) is a specific cell-surface marker for cancer cells and neovascular endothelial cells[15]. The VAP ($^{D}S^{D}N^{D}T^{D}R^{D}V^{D}A^{D}P$) peptide, presenting high affinity with GRP78, was reported possessing a well-demonstrated tumor cells binding and BTB penetration properties[16]. As one of benzamide analogues, *p*-hydroxybenzoic acid (pHA) has been proven an effective BBB-targeting moiety *via* the D1 and D2 dopamine receptors since 2011[17]. In our previous works, the "Y-shaped" peptide formed by two peptides connecting through aminocaproic acid were demonstrated possessing an increased modification density of targeting peptide. Herein, we synthesized the "Y-shaped" targeting material pHA-VAP (pVAP)-PEG-DSPE (Supporitng Information Fig. S1C), endowed with both the targeting functions of pHA and VAP, as previous works[16,18].

fdb 9.1.450/W UnicodeIn the present study, we fabricate a novel pVAP-decorated platelet membrane-hybrid liposome delivery system (pVAP-PL), with the model drug Cabazitaxel (CbTX) nanocrystal (CNC) loaded in through a film-rehydration and ultrasonic method (Fig. 1). The unique binding activities of activated platelet membranes in the hybrid liposomes (PL) were firstly confirmed. Then, the successful encapsulation of CNC into the pVAP-PL were characterized. The specific targeting properties of pVAP-PL/CNC were demonstrated thoroughly *in vitro* and *in vivo*. After one cycle of therapy, pVAP-PL/CNC eventually achieved the outperformance compared with the nondecorated PL/CNC and free drug both in 4T1 orthotopic and brain metastatic tumor models. All in all, in this work, we proposed an all-stage drug delivery platform for the therapy of brain metastatic TNBC leveraging the advantages of synthetic and natural targeting moieties.

2. Materials and methods

2.1. Cell lines and animals

4T1 breast cancer cells, HUVECs and bEnd.3 cells were purchased from Shanghai Institute of Cell Biology and cultured in the DMEM medium (Gibco, USA) supplemented with 10% FBS (Gibco, USA), 100 IU/mL penicillin (Gibco, USA), and 100 μg/mL streptomycin (Gibco, USA) at 37 °C in a humidified atmosphere containing 5% CO_2. BALB/c female mice were purchased from Shanghai SLAC Laboratory Animal Ltd. (China) with the age matched 6−8 weeks throughout all experiments. All the animal experiments were carried out according to the animal protocol approved by the Animal Ethics Committee of School of Pharmacy, Fudan University.

2.2. Preparation and characterization of platelet-hybrid liposomes

Human platelet membrane materials were derived from platelet-rich plasma through a repeated freeze-thaw process as previous report[19]. To prepare platelet-hybrid liposomes, the egg yolk lecithin (AVT Pharmaceutical Tech Co., Ltd., Shanghai, China), cholesterol (Sigma−Aldrich, USA) and DSPE-PEG_{2000} (LaysanBio, USA), with the 80:18:2 molar ratio, were dissolved in trichloromethane (Sinopharm Chem ical Reagent, China). After the solvent had been removed, the films were hydrated with PBS or PBS including platelet membranes (1:100 or 1:25, platelet membrane protein-to-lipid, *w*/*w*). Then, the conventional liposomes (Lip), platelet-hybrid liposomes (PL) and pure platelet membrane-derived vesicles (PV) were assembled through a sonication method (SCIENTZ, Ningbo, China). The DiO/DiD-labelled Lip, PL or PV were prepared with the same procedure except 0.2% (*w*/*w*) of DiO or DiD (Meilunbio, Dalian, China) mixing in the lipid.

The size and zeta potential of platelet, Lip, PL and PV were determined by dynamic light scattering (DLS) using a Malvern Nano ZS analyzer (Malvern, UK) ($n = 3$). The stability of different samples in PBS or after freeze drying were monitored by DLS, respectively ($n = 3$). To demonstrate the membrane fusion in PL, two lipophilic dyes, NBD-PE (Ex/Em: 463/536 nm) (Invitrogen, USA) and rhodamine DHPE (Ex/Em: 560/580 nm) (Invitrogen, USA) were employed to label the platelet membranes with 0.1% and 0.5% (*mol*/*mol*) final ratios of total membrane materials, respectively. Then liposome suspensions were added into the NBD-PE/rhodamine DHPE-doped platelet membrane materials at lipid to platelet membrane protein weight ratios of 200:1, 100:1, 50:1, 20:1 or 0:1, followed by a sonication for 5 min at 4 °C. The fluorescence spectrum of each sample was detected by a Tecan Infinite M200 Pro multiplate reader (BioTek, USA) using an excitation wavelength of 463 nm. To examine the total protein profile and specific membrane proteins in PL, the SDS-PAGE and western blotting assay were carried out with equivalent cell membranes and corresponding antibodies of GPVI (Abgent, USA), GPIIb/IIIa (Biolegend, USA), intergrin $\alpha 2$ (R&D, USA), GPIbα (R&D, USA), intergrin $\beta 1$ (R&D, USA) and CD47 (Invitrogen, USA).

2.3. Binding properties and pharmacokinetic behavior of platelet-hybrid liposomes

To assess the specific tumor cells targeting activity of PL, 4T1 breast cancer cells were seeded in 12-well plates at a density of 2×10^5 cells

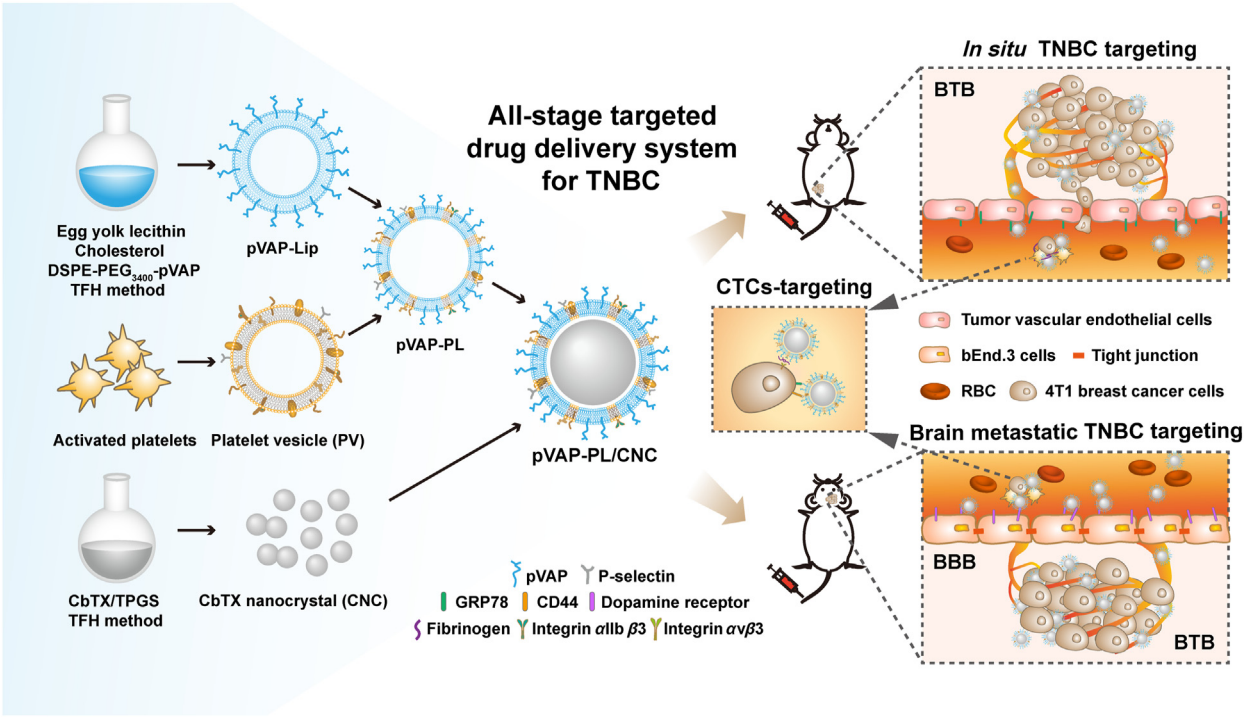

Figure 1 Schematic illustration of the preparation and targeting mechanism of the CNC-loaded pVAP-decorated platelet-membrane hybrid liposomes (pVAP-PL/CNC) for the all-stage targeted therapy of brain metastatic triple-negative breast cancer (TNBC). In brief, the pVAP-PL nanocarrier was developed using egg yolk lecithin, cholesterol, DSPE-PEG_{3400}-pVAP and activated platelet membranes through the thin-film hydration (TFH) method, then the CNC was loaded into pVAP-PL *via* ultrasonic method. The whole targeting processes of pVAP-PL/CNC to *in situ* TNBC, CTCs and brain metastatic lesions were obtained *via* the peptide pVAP and activated platelet membranes-mediated targeting delivery.

per well. Twenty-four hours later, 4T1 cells were treated with serum-free medium including 50 μg/mL of DiO-labelled Lip, PLL (PL-Low) (1:100, platelet membrane protein-to-lipid, *w*/*w*), PLH (PL-High) (1:25, platelet membrane protein-to-lipid, *w*/*w*) or PV at 4 °C for 30 min, respectively ($n = 3$). The binding results were analyzed by a laser scanning confocal microscope (ZEISS, Germany) and a flow cytometer (Beckman, USA) with the excitation/emission wavelength of 488/502 nm. To mimic the specific targeting of PLL or PLH to tumor cells under a physiological condition, the dynamic 4T1 tumor cells binding assay was performed as above except the tumor cells under a shear flow condition (188 s^{-1}) (Brookfield, USA)[20]. For the collagen or fibrinogen binding assay, 100 μg/mL of DiD-labelled Lip, PL (1:100, platelet membrane protein-to-lipid, *w*/*w*) and PV were added into collagen IV (Sigma−Aldrich, USA)- or fibrinogen (Sigma−Aldrich, USA)-precoated 96-well plates for 5 min ($n = 3$), respectively[21]. After washing three times with PBS, the retained samples were dissolved with DMSO (Meilunbio, Dalian, China), followed by qualitative and quantitative assay with an IVIS spectrum imaging system (PerkinElmer, USA) or multiplate reader (BioTek, USA) at the excitation/emission condition of 644/663 nm, respectively. Under a sheared condition, the collagen IV- or fibrinogen-precoated glass slides were put into the bottom of flow chamber (Naturethink, China) followed by 100 μg/mL of DiD-labelled Lip, PL (1:100, platelet membrane protein-to-lipid, *w*/*w*) or PV infusing at a shear rate of 500 s^{-1} for 30 min[22]. Different samples adhered to glass slides were observed and semi-quantitated under a fluorescence microscope (Leica, Japan) after a washing for 5 min.

For pharmacokinetic study, BALB/c mice were intravenously injected with 200 μL of DiD-labelled Lip, PLL, PLH or PV at a concentration of 2 mg/mL, respectively ($n = 5$). The blood samples were collected at preset time points (0.016, 0.16, 0.33, 0.66, 1, 2, 4, 8, 12 and 48 h) from mice eye socket vEin. The DiD-labelled samples were measured by a multiplate reader (BioTek).

2.4. *Preparation and characterization of DSPE-PEG_{3400}-VAP or DSPE-PEG_{3400}-pVAP*

The VAP ($^{D}S^{D}N^{D}T^{D}R^{D}V^{D}A^{D}PC$), pHA and pVAP ($^{D}S^{D}N^{D}T^{D}R^{D}V^{D}A^{D}PC$-Ahx-pHA) were synthesized by GL Biochem Ltd. (Shanghai, China). The DSPE-PEG_{3400}-VAP or DSPE-PEG_{3400}-pVAP was synthesized through covalent conjugation between thiolated peptide VAP or pVAP and DSPE-PEG_{3400}-Mal (LaysanBio, USA). In brief, the DSPE-PEG_{3400}-Mal was dissolved in DMF (Sinopharm Chemical Reagent, China) and then dropped into the peptide PBS (pH = 7.2) solution under a magnetic stirring condition (IKA, Germany). The reaction was monitored by HPLC (Agilent, USA). After that, the DSPE-PEG_{3400}-VAP or DSPE-PEG_{3400}-pVAP was purified through dialysis method (MWCO 3.5 kDa, Genestar, Shanghai, China) and confirmed by the disappearance of maleimide in the ChemNMR.

2.5. *Preparation and characterization of PL/CNC, VAP/CNC, pHA/CNC and pVAP/CNC*

CbTX and TPGS were dissolved into dichloromethane (Sinopharm Chemical Reagent, China) with a weight ratio of 1:1. Then, the CNC solution was obtained through a series of rotary evaporation (SENCO, Shanghai, China), hydration and sonication steps (KUDOS, Shanghai, China). The CNC-loaded PL, VAP-PL, pHA-

PL and pVAP-PL were prepared with the same procedure of PL above except that the PBS and DSPE-PEG_{2000} were replaced by CNC solution in hydration and DSPE-PEG_{3400}-VAP/DSPE-PEG_{3400}-pHA/DSPE-PEG_{3400}-pVAP in film formation, respectively. The fluorescent probe-labelled CNC were prepared with DiO/DiD/DiR incorporated at 0.2% (*w/w*). The size, zeta potential and stability in PBS at 4 °C of formulations were measured by DLS ($n = 3$). The samples treated with 2% sodium phosphotungstate (Aladdin, Shanghai, China) were observed by TEM (Hitachi, Japan). The lyophilized formulations were tested by PerkinElmer 1 DSC instrument (Waltham, MA, USA) for crystalline identification. The encapsulation efficiency (EE) of CNC in pVAP/CNC was calculated according to Eq. (1) after centrifugation (NACHT, Germany) and HPLC steps:

$$\mathrm{EE}\ (\%) = \frac{\mathrm{CNC_{total}} - \mathrm{CNC_{free}}}{\mathrm{CNC_{total}}} \times 100 \quad (1)$$

2.6. Drug release and pharmacokinetic study

One milliliter of CNC, PL/CNC, VAP/CNC or pVAP/CNC were added into dialysis bags (Genestar, Shanghai, China). Then the dialysis bags were placed in different release mediums (pH 7.4 and 6.5). Two hundred microliter of sample was replaced periodically under the condition of 65 rpm (IKA, Germany), 37 °C for 48 h ($n = 5$). The cumulated CbTX release amounts from each group were detected by HPLC.

BALB/c mice were intravenously injected with 200 μL of DiD-labelled CNC, PL/CNC, VAP/CNC or pVAP/CNC at a concentration of 1 mg/mL, respectively ($n = 5$). The blood samples were collected from mice eye socket vEin at preset time points (0.08, 0.25, 0.5, 1, 2, 4, 8, 16, 24 and 48 h).

2.7. Cellular uptake study

The cellular binding related markers of 4T1 cells (anti-CD44 antibody, CST, USA; anti-GRP78 antibody, CST, USA), HUVECs (anti-GRP78 antibody, CST, USA) and activated platelets (anti-P-selectin antibody, Absin, Shanghai, China) were identified by Western blotting assay through routine processes. 4T1 cells or HUVECs were seeded into 12-well plates or confocal dishes (NEST, Suzhou, China) at the density mentioned above. The cells were incubated by DMEM complete medium (Gibco, USA) including DiO-labelled Lip, PL/CNC, VAP/CNC or pVAP/CNC at a CbTX concentration of 5 μg/mL at 37 °C for 1.5 h ($n = 4$). The cellular uptake results were analyzed by a confocal microscope or FACS.

2.8. In vitro BBB/BTB models

For the BBB model, 100 μL of BCECs were seeded into 24-well Transwell at a density of 5×10^5 cells per chamber (0.4 μm polyester membrane, Corning, USA) with 600 μL of complete medium in each well. When the transendothelial electrical (Millicell ERS, Millipore, USA) resistance sustained over 200 Ω cm^2, DiD-labelled PL/CNC, pHA/CNC, pHA/CNC D+, pVAP/CNC or pVAP/CNC D+ were added into the chamber at a CbTX concentration of 100 μg/mL at 37 °C with 200 μL of sample collected from each well at 0.5, 1.5, 2.5 and 3.5 h, respectively ($n = 4$). For the BTB model, the BCECs were replaced by a co-culture of HUVECs and 4T1 cells at the density of 4×10^5 cells per chamber and 1×10^5 cells per well, respectively. When the BTB could be used, DiD-labelled PL/CNC, VAP/CNC, VAP/CNC V+, pVAP/CNC or pVAP/CNC V+ were added into the chamber as the same CbTX concentration of BBB assay above ($n = 4$). The transport amounts of formulations in each group across BBB or BTB were calculated through a multiplate reader.

2.9. 3D-tumor spheroids models

4T1 cells (1×10^6) were seeded into 6-well plates with the ultra-low attachment surface (Corning, USA). Ten days later, the 3D-tumor spheroids were removed to confocal dishes or Transwells for permeability studies. The tumor spheroids in dishes were incubated with DiO-labelled PL/CNC, VAP/CNC or pVAP/CNC at a CbTX concentration of 100 μg/mL at 37 °C for 1 h ($n = 4$). The same CbTX formulations with equal concentration above were added into Transwell chambers for 4 h. The fluorescence intensity and penetration depth of tumor spheroids were measured by a confocal microscope.

2.10. Endocytosis and exocytosis mechanism

4T1 cells were seeded into 12-well plates at the density mentioned above. For endocytosis mechanism investigation, the 4T1 cells were pretreated with anti-GRP78 antibody and different endocytosis inhibitors Chloropromazine, Filipin and Colchicine (Meilunbio, Dalian, China) at a concentration of 10 μg/mL for 0.5 h, respectively, then incubated with DiO-labelled PL/CNC, VAP/CNC or pVAP/CNC at a CbTX concentration of 20 μg/mL at 37 °C for 1.5 h ($n = 4$). For exocytosis mechanism research, the 4T1 cells were pre-incubated with DiO-labelled PL/CNC, VAP/CNC or pVAP/CNC at a concentration of 20 μg/mL at 37 °C for 3 h. Then different exocytosis inhibitors Nocodazole, Monensin and Brefeldin A (Meilunbio, Dalian, China) were added into the culture medium at a concentration of 10 μg/mL for 3 h, respectively ($n = 4$)[23–25]. The cellular uptake results were analyzed by a FACS.

2.11. Cytotoxicity study

4T1 cells or HUVECs were seeded into 96-well plates with a density of 500 or 2000 cells per well, respectively. Different formulations with CbTX concentrations ranging from 10 pg/mL to 10 μg/mL were added at 37 °C for 48 h ($n = 5$). Further steps of MTT assay (Meilunbio, Dalian, China) were conducted according to a routine protocol.

2.12. Cell migration assay

4T1 cells with defined cell-free gaps were prepared through the wound healing inserts (Ibidi, USA), followed by an incubation with CbTX, PL/CNC, VAP/CNC or pVAP/CNC at a CbTX concentration of 50 ng/mL for 48 h ($n = 4$). The cell migration in different groups were measured and calculated through an Image J 1.53e software (USA).

2.13. Orthotopic breast cancer targeting and in vivo biodistribution

4T1-luc cells (4×10^6) were inoculated into the mammary fat pad of BALB/c mice to establish the orthotopic breast cancer models. Fourteen days later, DiR- or DiD-labelled PL/CNC, VAP/CNC or pVAP/CNC were injected into mice *via* tail vein at a dose of

8 mg/kg animal weight. NIR fluorescent images of mice, major organs and tumors were obtained using an IVIS Imaging System under the excitation/emission wavelength of 745/780 nm ($n = 4$). The radiant efficiency of each formulation was evaluated by the fluorescent value in the tumor area. The semiquantified and quantified results were detected by a microplate reader or HPLC after the tissue homogenization (SKSI Tissue Lyser, BiHeng Biotechnology Co., Ltd., Shanghai, China) ($n = 4$), respectively. The tumors harvested at 24 h after injection were embedded in OTC (SAKURA, USA) for frozen sections (5 μm). The localization of GRP78 with different DiD-labelled formulations were observed by a confocal microscope.

2.14. Brain metastatic breast cancer targeting

4T1-luc cells were implanted into the right striatum of mice at a density of 5×10^5 guided by a Stereotaxic Instruments (RWD, Shenzhen, China)[26]. Two weeks after inoculation, the mice intravenously received different DiR- or DiD-labelled CbTX formulations (PL/CNC, VAP/CNC, pHA/CNC or pVAP/CNC) at the same dose above (8 mg/kg) ($n = 3$). The NIR fluorescent images, semiquantification and quantification of DiR-labelled formulations in the brain were measured as mentioned before. The frozen sections of brain tissues were performed 24 h following injection.

2.15. Anti-orthotopic breast tumor and brain metastases efficiency

The 4T1 orthotopic breast cancer models ($n = 6$) and corresponding brain metastasis models ($n = 10$) were established as described above. The mice randomly received one cycle (Days 8, 11 and 14 following inoculation) of therapy with saline, CbTX, PL/CNC, VAP/CNC and pVAP/CNC or saline, CbTX, PL/CNC, VAP/CNC, pHA/CNC and pVAP/CNC at a CbTX dose of 6 mg/kg, respectively. The animal weight and tumor volume were measured every two days. The *in situ* tumor volume (V), *in situ* tumor suppression (TS) ratio and therapeutic index (TI) were calculated according to Eqs. (2)−(4), respectively[10,27]:

$$V = \frac{\text{Length} \times \text{Width}^2}{2} \tag{2}$$

$$\text{TS}\,(\%) = \left(1 - \frac{V_t}{V_{t0}}\right) \times 100 \tag{3}$$

$$\text{TI} = \frac{1 - \frac{W_t}{W_{t0}}}{1 - \frac{W_b}{W_{b0}}} \tag{4}$$

The orthotopic tumor tissues or brain tissues harvested one week after last administration were used for paraffin section with a H&E, CD31 (anti-CD31 antibody, Servicebio, China) and TUNEL (TUNEL FITC Apoptosis Detection Kit, Vazyme, China) staining assay, respectively. The positive results of $CD31^+$ or TUNEL+ in slices were analyzed by Image J software ($n = 3$).

2.16. Biosafety evaluation

The whole blood and serum samples of BALB/c mice which received one time delivery of saline, CbTX, PL/CNC, VAP/CNC or pVAP/CNC at the treatment dose of 6 mg/kg were subjected to hematological and biochemical analysis. The major organs of each mouse above were subsequently collected for pathological section and GFAP (anti-GFAP antibody, Abcam, UK) staining assay.

3. Results and discussion

3.1. Preparation and characterization of platelet membrane-hybrid liposomes

The unloaded platelet membrane-hybrid liposomes (PL) were prepared through a thin film-hydration method with 1% (*w*/*w*) of activated platelet membrane materials added during the step of hydration. The PL presented a median diameter (98 nm) and surface charge value (−31.8 mV) between the Lip and PV (Supporting Information Fig. S2A and S2B). The stability of PL in PBS and after a freeze-drying indicated that platelet membranes could integrate with general lipids to form stable liposomes (Fig. S2C and S2D). The fusion of platelet membranes with general lipids was based on the rearrangement of lipid molecules under an ultrasonic condition. In order to evaluate the fusion of platelet membranes with lipids, the FRET assay was conducted. The recovered fluorescence emission from the platelet membrane materials at 534 nm along with an increasingly mixed lipids suggested the successful fusion of two kinds of materials (Fig. S2E). The incorporated platelet membranes in PL retained a similar whole protein profile as the activated platelets and pure platelet vesicles (PV) (Fig. S2F), with a slight loss of specific protein (GPVI, GPIIb/IIIa, intergrin α2, GPIbα, intergrin β1 and shared protein CD47) after the fusion step (Fig. S2G and S2H).

After characterizing the integrality of platelet membranes in PL, tumor metastasis-related functions of platelet membranes were evaluated. To optimize the input-ratio of membrane materials, the PL was divided into two groups (PLL and PLH) with 1% (*w*/*w*) or 4% (*w*/*w*) of platelet membranes mixed. According to the binding effect of PLL to 4T1 breast cancer cells under a static or sheared condition (Supporting Information Fig. S3A−S3C) and its nearer conventional liposome-like long-circulation behavior *in vivo* (Fig. S3D), the formulation of PLL was chosen for further studies. The near-infrared (NIR) imaging and fluorescence images indicated that the PL still retained the binding activities to collagen and fibrinogen like PV under a static condition (Fig. S3E and S3F) or physiological shear flow (Fig. S3G and S3H). Moreover, the PL showed a superior binding advantage under the sheared environment (Fig. S3K and S3L) as compared with the static condition (Fig. S3I and S3J).

3.2. Preparation and characterization of PL/CNC, VAP/CNC and pVAP/CNC

The CNC was fabricated through a film-rehydration method with 50% (*w*/*w*) of Tocofersolan (TPGS) mixed[28]. The DSPE-PEG_{3400}-VAP and DSPE-PEG_{3400}-pVAP were synthesized through the covalent conjugation between thiolated peptide VAP or pVAP and Mal-PEG_{3400}-DSPE, respectively. The characterizations of DSPE-PEG_{3400}-VAP and DSPE-PEG_{3400}-pVAP were shown in Fig. S1A and S1B (Varian, USA). The molar ratio of DSPE-PEG_{3400}-VAP or DSPE-PEG_{3400}-pVAP in VAP peptide-decorated PL (VAP-PL) or pVAP peptide-decorated PL (pVAP-PL) was 2%. The encapsulation of CNC into PL, VAP-PL or pVAP-PL (abbreviated to PL/CNC, VAP/CNC and pVAP/CNC) were carried out during the step of hydration. The drug-loading of CbTX in pVAP/CNC was about 14.3%. The encapsulation

efficiency of CNC in pVAP/CNC was approximately 96.6%. After coating with PL or pVAP-PL membrane materials, the size of resulting formulations changed from 116 nm to 133.8 or 155 nm and the corresponding zeta potential changed from −15.0 to −20.5 or −15.5 mV (Fig. 2A–C). When visualized under a transmission electron microscopy (TEM), the core-shell structures were obviously displayed in the PL/CNC, VAP/CNC and pVAP/CNC (Fig. 2D). The PL/CNC, VAP/CNC and pVAP/CNC exhibited similar crystalline states in the Differential L Scanning Caborimetry (DSC) thermograms, which were different from that of CNC or CbTX (Fig. 2F). Additionally, as compared with CNC, the PBS stabilities of PL/CNC, VAP/CNC and pVAP/CNC were visibly improved (Fig. 2E). All these results taken together suggested that the CNC was successfully loaded in.

3.3. *Drug release and pharmacokinetic study*

To explore the effect of hybrid membrane materials on drug release, the amounts of drug release in different groups were monitored at preset times. The drug release mechanism from CNC was thought to be dissolution and diffusion. We found that the fusion membrane materials distinctly decelerated the release of CbTX from the PL/CNC, VAP/CNC or pVAP/CNC compared with CNC (Fig. 2G) in the PBS at pH 7.4. The cumulative release amounts of CbTX in pVAP/CNC and CNC groups at 48 h were 64.53% and 84.0%, respectively (PBS at pH 7.4). Combining with the stability results in Fig. 2E, the relatively lower drug release in pVAP group might be due to the better stability of pVAP than CNC. When turning to the PBS at pH 6.4, the cumulative release percentages in different groups were similar. The cumulative release amount of CbTX from pVAP/CNC reached 77% at 48 h.

For the research of *in vivo* circulation behavior, the DiD-labelled formulations were administered *via* tail vein. The pharmacokinetic parameters were summarized in Table 1. As shown in Fig. 2H, the blood circulation curves of PL/CNC, VAP/CNC and pVAP/CNC were higher than that of CNC, with the pharmacokinetic parameters $t_{1/2\alpha}$ and AUC_{0-48h} of pVAP/CNC (0.43 h and 1561.27 mg/L·h) improved as compared with that of CNC (0.23 h and 1080.20 mg/L·h). Combining with the results of drug release and pharmacokinetic study, we speculated that coating with the hybrid membrane materials pVAP-PL might help to improve the targeting efficiency of drug delivery system pVAP-PL/CNC through avoiding the early release of CbTX and prolonging the *in vivo* circulation time of CNC.

3.4. *Cellular and BBB/BTB targeting of pVAP/CNC*

To verify the cellular targeting ability of pVAP/CNC, targeting related cell membrane markers GRP78, CD44 and P-selectin were identified through a Western blotting assay (Fig. 3C). High-expression of GRP78 was shown both on the surface of 4T1 breast cancer cells and HUVECs, providing the dual-targets of VAP peptides in this study. The expression of CD44 and P-selectin on 4T1 cells and PL were validated, respectively, laying the foundation of platelet membrane-based targeting to tumor cells. After the incubation with the DiO-labelled Lip/CNC or PL/CNC at a CbTX dose of 5 μg/mL at 37 °C for 1.5 h, we found that obviously more PL/CNC (2.7 folds of Lip) were taken into 4T1 cells, indicating an excellent targeting ability of the PL/CNC to 4T1 tumor cells (Fig. 3A and B). Interestingly, the cellular intake gap between the PL/CNC and Lip/CNC was lessened as compared to that of PL and Lip, which might be attributed to the improved rigidity of PL/CNC and Lip/CNC after the CNC loaded in. To confirm the specific targeting of pVAP/CNC, 4T1 cells and HUVECs were incubated with the same dose of DiO-labelled PL/CNC, VAP/CNC or pVAP/CNC at the conditions above. Showing qualitative cellular internalization results of pVAP/CNC > VAP/CNC > PL/CNC in 4T1 cells (Fig. 3J) and HUVECs (Fig. 3K), the quantitative analysis of FACS further demonstrated the significant targeting advantage of pVAP/CNC, with the 3.4-or 4.7-fold intake of PL/CNC against 4T1 cells (Fig. 3D and E) or HUVECs (Fig. 3G and H), respectively.

To access the bio-barrier transport efficiency of formulations in this study, the *in vitro* BBB and BTB models were established as previous works[15,29]. The BBB or BTB monolayers were incubated with 100 μg/mL of DiD-labelled PL/CNC, pHA/CNC, pHA/CNC+dopamine (pHA/CNC D+), pVAP/CNC and pVAP/CNC+dopamine (pVAP/CNC D+) or PL/CNC, VAP/CNC, VAP/CNC+VAP peptide (VAP/CNC V+), pVAP/CNC and pVAP/CNC+VAP peptide (pVAP/CNC V+) at 37 °C for 3.5 h, respectively. The accumulated transport amounts in Fig. 3F and I indicated that the "Y-shaped" peptide-modified formulation pVAP/CNC held an obvious BBB or BTB transport advantage over the PL/CNC. While, the transport amounts in VAP/CNC and pVAP/CNC groups in Fig. 3I hinted a potential expression of dopamine receptors on HUVECs.

3.5. *Penetration of pVAP/CNC (after transport across BTB) into 3D-tumor spheroids*

To evaluate the penetration property of pVAP/CNC into tumor tissues, 4T1 3D-tumor spheroids were cultivated according to previous work and incubated with 100 μg/mL of DiO-labelled PL/CNC, VAP/CNC or pVAP/CNC[29]. As shown in the fluorescent multi-level scan images (Fig. 4A), the tumor spheroid profiles in x/y/z direction (Fig. 4B) and the fluorescence intensity from tumor spheroid interior to surface (Fig. 4C), the pVAP/CNC displayed a remarkable penetration superiority than PL/CNC both in fluorescence intensity and penetration depth. Interestingly, the fluorescence intensity in VAP/CNC was marginally higher than that of pVAP/CNC. But when transporting across the BTB, the VAP/CNC and pVAP/CNC groups exhibited similar fluorescence intensity (Fig. 4D) and penetration depth (Fig. 4E and F), which might be explained by the BTB results in Fig. 3I.

To explore the VAP-mediated penetration of VAP/CNC and pVAP/CNC deep into 3D-tumor spheroids, the endocytosis and exocytosis mechanism of PL/CNC, VAP/CNC and pVAP/CNC were investigated *via* 4T1 tumor cells treated with corresponding inhibitors, respectively. As shown in Fig. 4G, the unaffected cellular uptake of PL/CNC suggested its membrane fusion way into tumor cells. While, the anti-GRP78-, Chloropromazine- and Filipin-mediated reduction of relative intracellular fluorescence intensity in VAP/CNC and pVAP/CNC groups indicated the GRP78 receptor-, clathrin- and caveolin-mediated endocytosis mechanism of VAP/CNC and pVAP/CNC. As shown in Fig. 4H, the Nocodazole-mediated increase of relative intracellular fluorescence intensity in PL/CNC group suggested that the internalized particles mostly accumulated in the lysosomal. However, the Monensin-mediated increase of relative intracellular fluorescence intensity in VAP/CNC and pVAP/CNC groups revealed that the endosome secretion was the main exocytosis pathway of VAP/CNC and pVAP/CNC. Therefore, we speculated that the superior

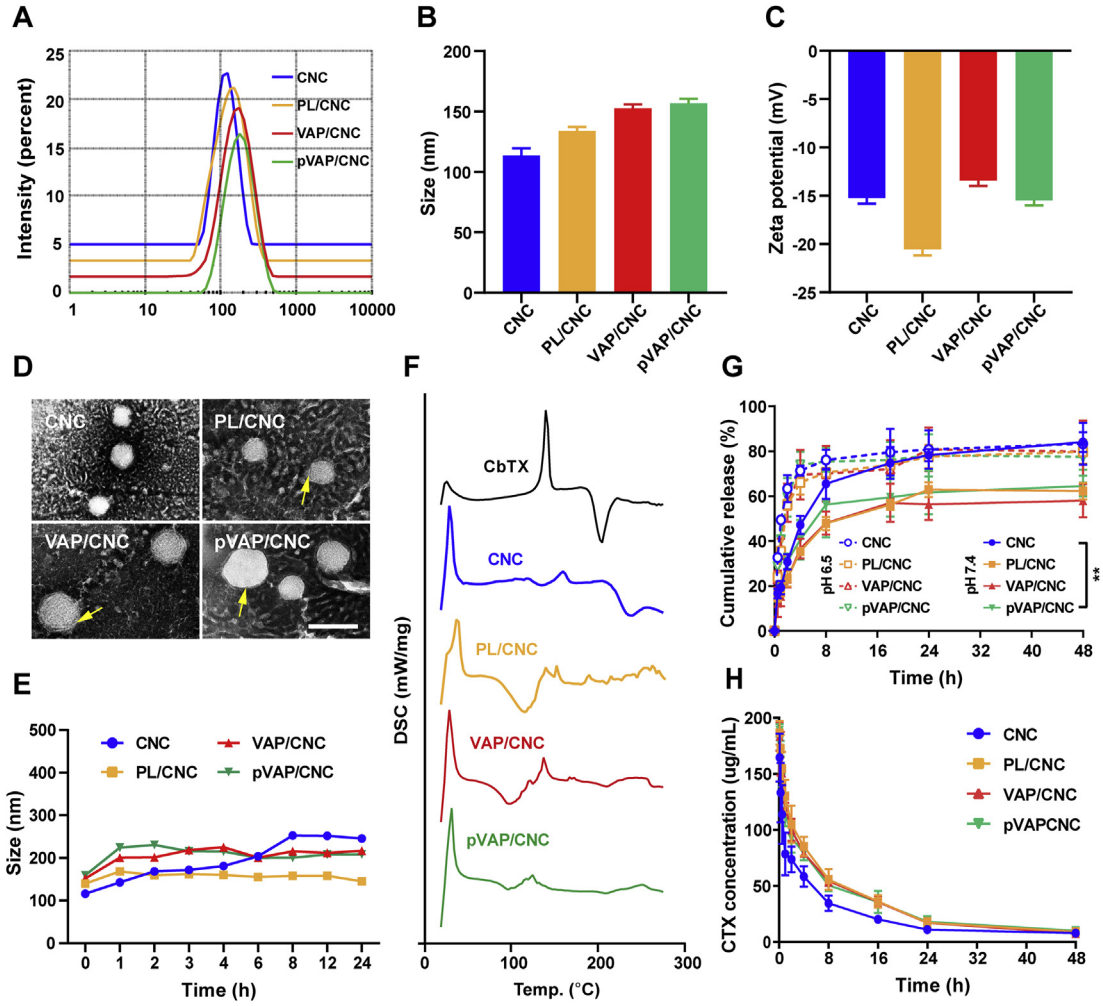

Figure 2 Characterization of pVAP/CNC. Size (A and B), zeta potential (C), TEM image (D) and stability in PBS (E) of pVAP/CNC ($n = 3$; mean ± SD). The arrows indicated the membrane materials around CNC. (F) DSC thermogram of pVAP/CNC. (G) Drug release from pVAP/CNC at pH 7.4 and 6.5 ($n = 5$; mean ± SD). (H) Pharmacokinetic profile of pVAP/CNC ($n = 5$; mean ± SD). Scale bar = 100 nm $^{**}P < 0.01$, one-way ANOVA.

penetration abilities of VAP/CNC and pVAP/CNC than PL/CNC into 3D-tumor spheroids might be due to the VAP-mediated endocytosis and exocytosis mechanism.

3.6. *In vitro anti-tumor activity of pVAP/CNC*

The cytotoxicity of pVAP/CNC against 4T1 cells and HUVECs were tested by MTT assay. After the incubation of CbTX, PL/CNC, VAP/CNC or pVAP/CNC at a range of CbTX concentrations from 10 pg/mL to 10 μg/mL for 48 h, the cell viability of 4T1 cells and HUVECs were shown in Fig. 5A and B, with the corresponding IC_{50} values of pVAP/CNC reduced 25.5 folds (Fig. 5C) and 1.6 folds (Fig. 5D) as compared with that of PL/CNC, respectively.

To investigate the anti-metastasis ability of pVAP/CNC *in vitro*, cell migration assay was performed using the wound healing inserts (Ibidi). The 4T1 cells in pVAP/CNC group exhibited a most conspicuous inhibition of migration with the minimal reduction of cell-free gap among all treatment groups at 48 h (Fig. 5E). As shown in Fig. 5F, the migration rate of pVAP/CNC decreased to about one-fourth or one-third of that of CbTX or PL/CNC, respectively. All these evidences above indicated that

Table 1 The pharmacokinetic parameters of different CbTX formulations.

Treatment	$t_{1/2\alpha}$ (h)	AUC_{0-48h} (mg/L·h)	C_{max} (mg/L)
CNC	0.23±0.22	1080.20±137.99	164.55±21.32
PL/CNC	0.42±0.23*	1661.04±301.91*	186.51±10.49*
VAP/CNC	0.43±0.19*	1562.49±5.82*	183.56±12.98*
pVAP/CNC	0.43±0.13*	1561.27±281.48*	188.51±5.56*

Data are presented as mean±SD ($n = 5$).
*P<0.05, compared with CNC.

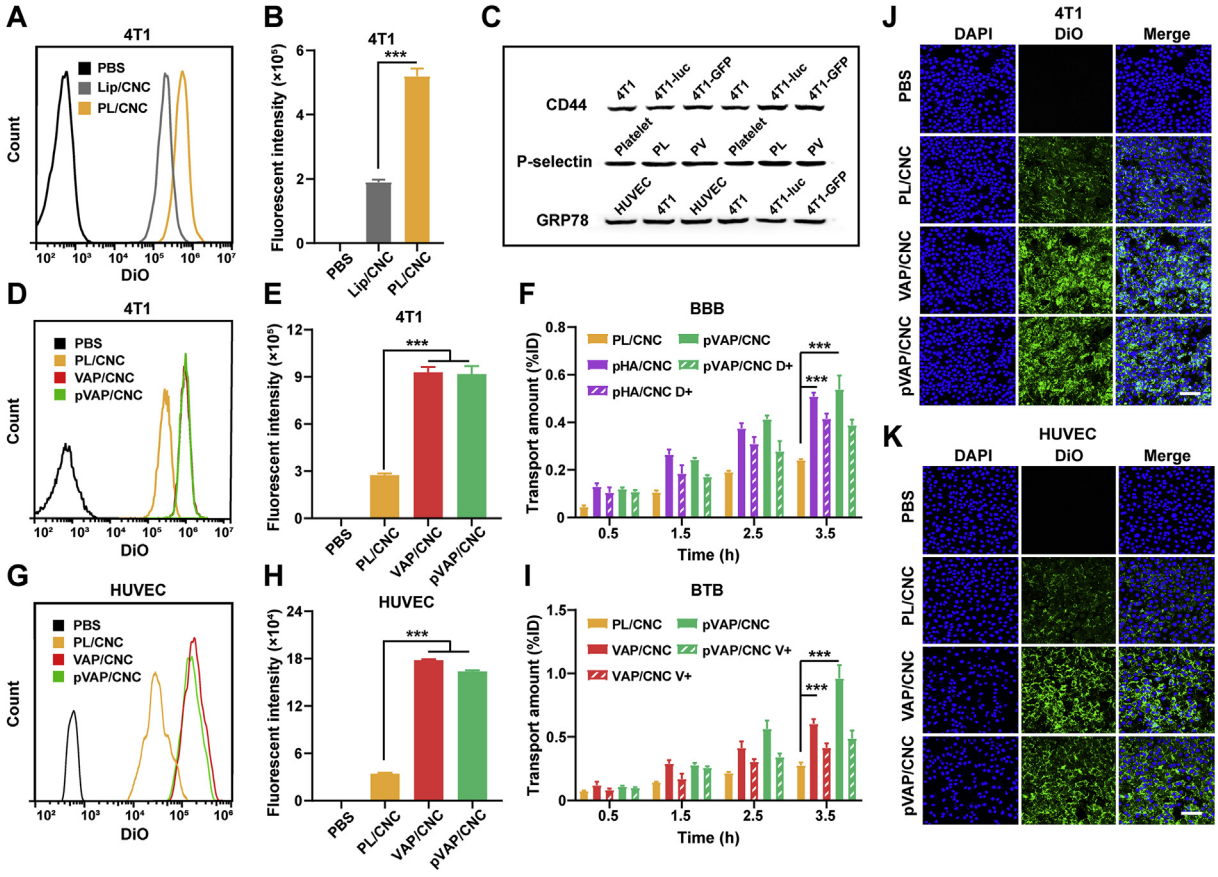

Figure 3 Cellular and BBB/BTB targeting of pVAP/CNC. Flow cytometry histograms (A) and quantification results (B) of 4T1 cells treated with PBS, Lip/CNC or PL/CNC at a CbTX concentration of 5 μg/mL at 37 °C for 1.5 h. (C) Western blotting results of the cellular targeting related markers (CD44, P-selectin, GRP78). Flow cytometry histograms (D) and quantification results (E) of 4T1 cells treated with PBS, PL/CNC, VAP/CNC or pVAP/CNC at a CbTX concentration of 5 μg/mL at 37 °C for 1.5 h. (G) and (H) were cellular uptake results of HUVECs performed as 4T1 cells. (F) The BBB transport amounts of PL/CNC, pHA/CNC, pHA/CNC D+ (dopamine+), pVAP/CNC or pVAP/CNC D+ (dopamine+) at a CbTX dose of 100 μg/mL at 37 °C with 200 μL of sample collected at 0.5, 1.5, 2.5 and 3.5 h, respectively. (I) The BTB transport amounts of PL/CNC, VAP/CNC, VAP/CNC V+ (VAP peptide+), pVAP/CNC or pVAP/CNC V+ (VAP peptide+) with the same CbTX dose and sample collection steps as (F). Confocal images of 4T1 cells (J) and HUVECs (K) incubated with PBS, PL/CNC, VAP/CNC or pVAP/CNC at a CbTX concentration of 5 μg/mL at 37 °C for 1.5 h. Scale bar = 100 μm. Data are presented as mean ± SD ($n = 4$). ***$P < 0.001$, one-way ANOVA.

the pVAP/CNC possessed an excellent suppressive activity in tumor proliferation and migration at the cellular level.

3.7. *Orthotopic breast tumor targeting and in vivo biodistribution*

To explore the preferential targeting property of pVAP/CNC in orthotopic breast tumor models, the NIR imaging of DiR-labelled PL/CNC, VAP/CNC and pVAP/CNC were carried out 14 days following implantation. The higher accumulation of pVAP/CNC than PL/CNC in tumor tissues were exhibited in Fig. 6A. The corresponding radiant efficiency (Fig. 6B) and semi-quantitative results (Fig. 6C) of PL/CNC, VAP/CNC and pVAP/CNC in tumor tissues were analyzed at preset times. Additionally, the quantitative biodistribution of each formulation in major organs and tumor tissues were evaluated by the CbTX content per gram of tissues. The PL/CNC, VAP/CNC and pVAP/CNC were mainly distributed in the liver and spleen, which was in accord with the distribution characteristic of traditional nanoparticles. The quantitative results of different CbTX formulations accumulated in the tumor and brain tissues demonstrated the specific targeting advantage of pVAP/CNC to orthotopic breast tumors and brain tissues. The colocalization of DiD-labelled pVAP/CNC and GRP78 in frozen tumor tissues (Fig. 6D) further provided an intuitive support to the preponderant accumulation of pVAP/CNC in 4T1 *in situ* tumors. The higher fluorescent signal in VAP/CNC group in Fig. 6A and the slight difference of the radiant efficiency (Fig. 6B) and semi-quantitative results (Fig. 6C) between the VAP/CNC and pVAP/CNC groups might be due to the different fluorescence statistical methods. Compared with the fluorescent signal in Fig. 6A and B, the fluorescent signal (Fig. 6C) and CbTX content (Fig. 6D and E) calculated after a tissue homogenate revealed the distribution of each formulation in the total tumor tissues.

3.8. *Anti-in situ breast cancer efficiency*

To assess the anti-*in situ* breast cancer efficiency, the 4T1 tumor volumes of each group were monitored every two days during the drug delivery cycle. The tumors in pVAP/CNC therapeutic group were markedly inhibited with the tumor volumes only about one-third even a quarter of that in PL/CNC and CbTX groups on Day

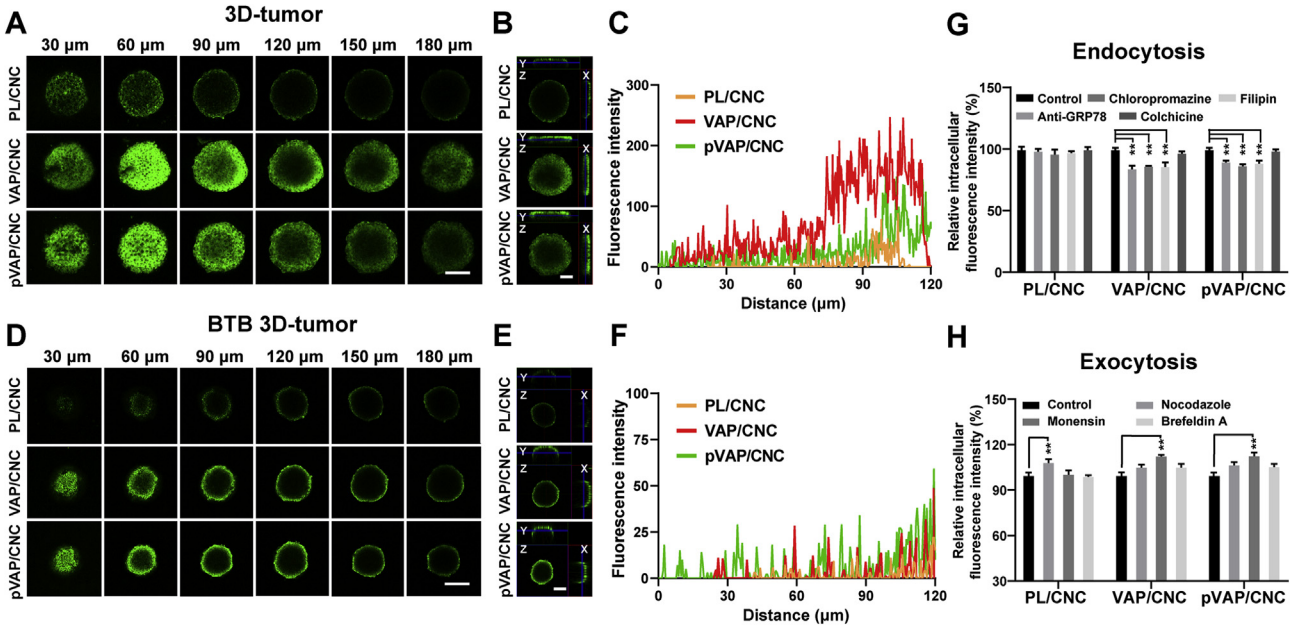

Figure 4 Penetration of pVAP/CNC into 3D-tumor spheroids. Multi-level scan images with an interval of 30 μm (A) and profiles in X/Y/Z direction (B) of 4T1 3D-tumor spheroids incubated with PL/CNC, VAP/CNC or pVAP/CNC at a CbTX dose of 100 μg/mL at 37 °C for 1 h. (C) The fluorescence intensity from the interior to the surface of the tumor spheroids in (A). (D) The confocal images of the PL/CNC, VAP/CNC or pVAP/CNC penetrated into the 4T1 3D-tumor spheroids after across BTB with the same CbTX dose as (A). (E) The profiles in X/Y/Z direction of tumor spheroids in (D). (F) The fluorescence intensity from the interior to the surface of the tumor spheroids in (D). (G) The relative cellular uptake efficiency of PL/CNC, VAP/CNC and pVAP/CNC into 4T1 tumor cells after a pretreatment with various endocytosis inhibitors. (H) The relative 4T1 intracellular fluorescence intensity of PL/CNC, VAP/CNC and pVAP/CNC following a pretreatment with various exocytosis inhibitors. Scale bar = 100 μm. Data are presented as mean ± SD ($n = 4$). $^{**}P < 0.01$, one-way ANOVA.

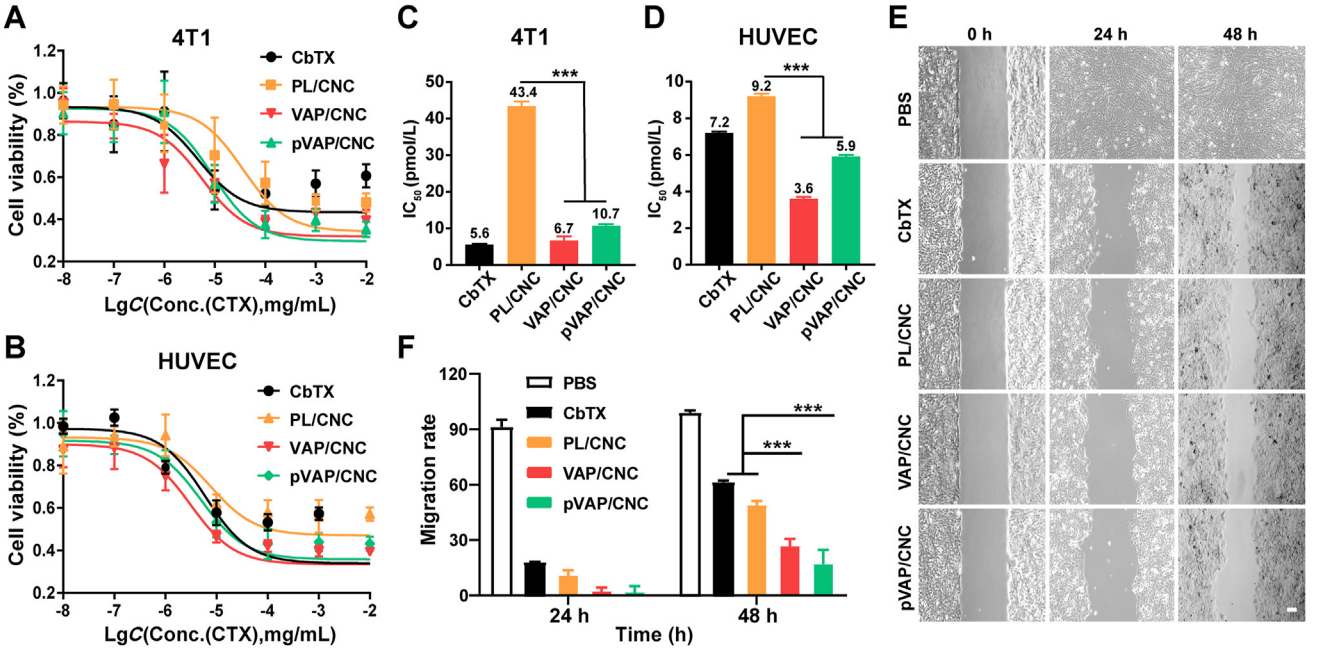

Figure 5 *In vitro* anti-tumor activity of pVAP/CNC. Viability of 4T1 cells (A) and HUVECs (B) incubated with CbTX, PL/CNC, VAP/CNC or pVAP/CNC at a CbTX concentration ranging from 10 pg/mL to 10 μg/mL for 48 h ($n = 5$; mean ± SD). The IC_{50} values of CbTX formulations against 4T1 cells (C) and HUVECs (D). (E) The 4T1 cells migration treated with CbTX, PL/CNC, VAP/CNC or pVAP/CNC at a CbTX dose of 50 ng/mL for 48 h ($n = 4$, mean ± SD). (F) The migration rate of different CbTX formulations in (E). Scale bar = 50 μm $^{***}P < 0.001$, one-way ANOVA.

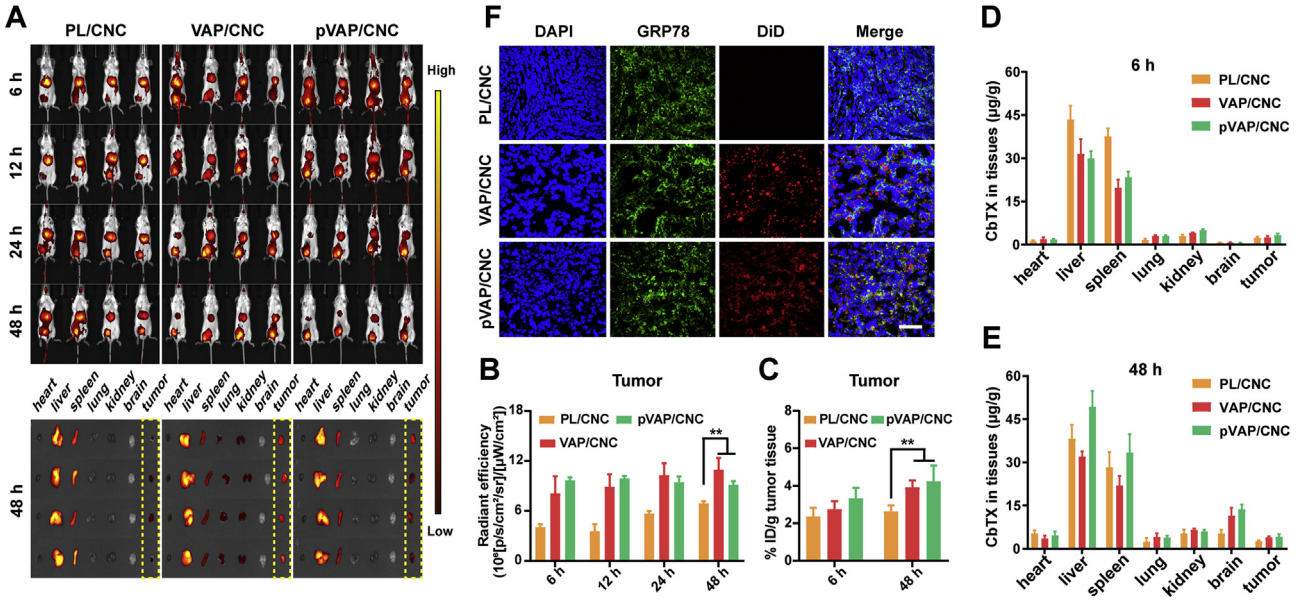

Figure 6 Orthotopic breast tumor targeting and biodistribution. (A) *In vivo* NIR imaging of 4T1-orthotopic tumor-bearing mice administrated with PL/CNC, VAP/CNC or pVAP/CNC at a CbTX dose of 8 mg/kg *via* tail vein. The *ex vivo* images of major organs and tumor tissues were harvested 48 h following administration. (B) The radiant efficiency of different formulations in tumor tissues in (A). (C) The semiquantitative assay of PL/CNC, VAP/CNC and pVAP/CNC in tumor tissues after the tissue homogenate. The *in vivo* biodistribution of PL/CNC, VAP/CNC and pVAP/CNC in major organs and tumor tissues at 6 h (D) and 48 h (E) following administration with a same dose of (A). (F) The confocal images of tumor tissues in PL/CNC, VAP/CNC and pVAP/CNC groups collected 24 h following administration with a same dose of (A). Blue: cell nuclei; green: GRP78; red: DiD-labelled CbTX formulations; scale bar = 100 μm. Data are presented as mean ± SD ($n = 4$). $^{**}P < 0.01$, one-way ANOVA.

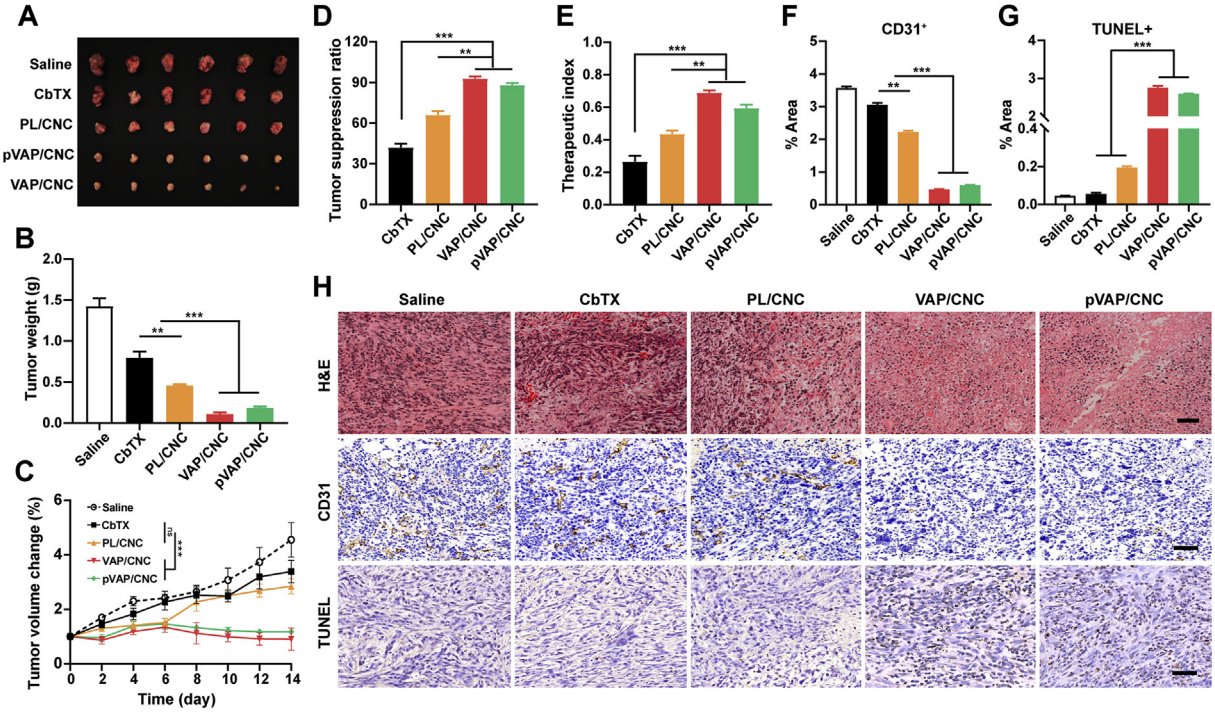

Figure 7 Anti-*in situ* breast cancer efficiency. The images (A) and tumor weight (B) of 4T1 *in situ* tumors after one cycle of treatment with saline, CbTX, PL/CNC, VAP/CNC or pVAP/CNC at a total CbTX dose of 18 mg/kg ($n = 6$; mean ± SD). (C) The tumor volume changes during the treatment cycle ($n = 6$; mean ± SD). The tumor suppression ratio (D) and therapeutic index (E) of different therapeutic groups ($n = 6$; mean ± SD). (H) The H&E, CD31 and TUNEL staining assay of different therapeutic groups. The area percentage of $CD31^+$ (F) and TUNEL+ (G) in (H) ($n = 3$; mean ± SD). Scale bar = 50 μm $^{**}P < 0.01$, $^{***}P < 0.001$, one-way ANOVA.

15 following implantation (Fig. 7A and C). The corresponding tumor weight was measured, showing that the tumor weight treated with pVAP/CNC reduced 2.5- and 4.3-fold from that in PL/CNC and CbTX groups (Fig. 7B). Ultimately, the pVAP/CNC obtained the 1.4- or 2.2-fold tumor suppression ratio and 1.5- or 2.5-fold therapeutic index of that in PL/CNC or CbTX treatment groups. The anti-orthotopic tumor effect of pVAP/CNC were further evaluated from the histological level. Sections of tumor tissues were stained with H&E, TUNEL and CD31 to assess the necrosis, apoptosis and angiogenesis. In H&E staining assay, relatively sparse cell nucleus and more obviously pyknosis and karyorrhexis were observed in the pVAP/CNC group as compared to that in PL/CNC and CbTX groups (Fig. 7H). The pVAP/CNC induced a significant apoptosis (Fig. 7G and H) and inhibition of angiogenesis (Fig. 7F and H) in comparison to PL/CNC and CbTX. All these results indicated that the formulation pVAP/CNC achieved a remarkably enhanced anti-orthotopic breast tumor effect after the modification of pVAP peptide. While, the slightly better anti-tumor effect of VAP/CNC in Fig. 7 might be attributed to the partial specific accumulation of pVAP/CNC in the brain.

3.9. Brain metastatic breast cancer targeting and anti-metastasis activity

Encouraged by the excellent antitumor effects of pVAP/CNC in orthotopic breast tumor models, the 4T1 brain metastasis models were established to explore the brain targeting capability and anti-brain metastasis efficacy of pVAP/CNC. The *in vivo* NIR-images (Fig. 8A) along with corresponding fluorescent semiquantitative (Fig. 8B) and quantitative results (Fig. 8C) of brain tissues showed that the decoration of pVAP peptide significantly improved the specific accumulation in the brain. As shown in Fig. 8D, the pVAP/CNC exhibited the most extensive distribution in the brain metastatic tissues, which further confirmed the superiority of "Y-shaped" peptide pVAP compared with the single targeting moiety VAP or pHA in the brain metastasis targeting delivery. After receiving one cycle of therapy with saline, CbTX, PL/CNC, VAP/CNC, pHA/CNC or pVAP/CNC at the same dose in anti-orthotopic tumors above, the anti-brain metastasis effects were intuitively reflected by animal survival times and histologic sections of the brain. As shown in Fig. 9A, the median survival times of CbTX (20 days), PL/CNC (21 days), VAP/CNC (24 days), pHA/CNC (21.5 days) and pVAP/CNC (33 days) groups were prolonged step by step following the CNC being encapsulated into hybrid-liposome and modified with targeting peptides. The increase in survival time (IST) of pVAP/CNC were improved to 7.5-fold of that of CbTX, with one-fifth of mice still being alive on Day 45 following inoculation. The pVAP/CNC mediated the most obvious brain metastasis suppressive effect, showing a minimum area of metastatic lesions (Fig. 9B) and the lowest expression of CD31 (Fig. 9B and C) in tumor tissues, whereas the CbTX exhibited a negligible therapeutic effect (Fig. 9B). Although the

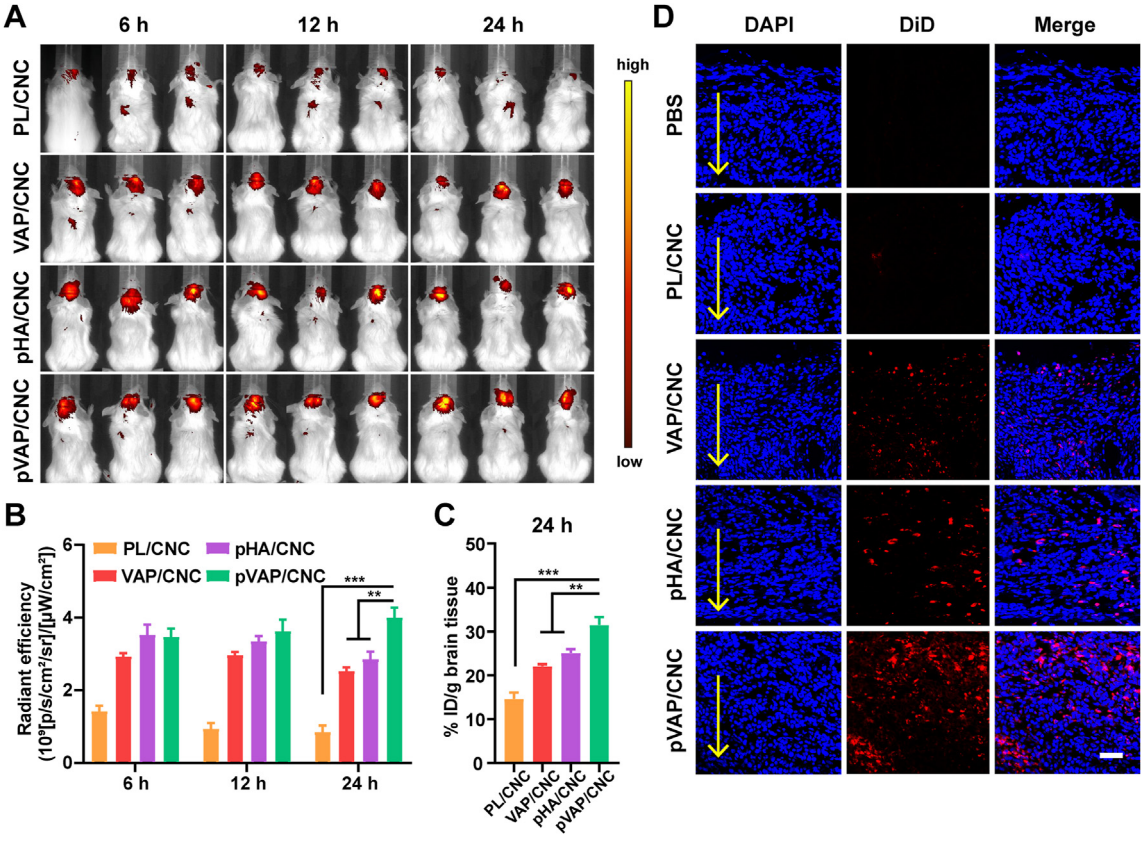

Figure 8 Brain metastatic breast cancer targeting. (A) *In vivo* NIR imaging of 4T1-brain metastatic tumors administrated with PL/CNC, VAP/CNC, pHA/CNC or pVAP/CNC at a CbTX dose of 8 mg/kg *via* tail vein. (B) The radiant efficiency of different formulations in the brain tissues in (A). (C) Fluorescent quantification of different formulations in the brain tissues 24 h after administration. (D) Confocal images of brain metastatic tumor tissues in PL/CNC, VAP/CNC, pHA/CNC and pVAP/CNC groups collected 24 h after administration with the same dose of (A). Blue: cell nuclei; red: DiD-labelled CbTX formulations; arrows indicated the depth of tumor tissues; scale bar = 100 μm. Data are presented as mean ± SD ($n = 3$). $^{**}P < 0.01$, $^{***}P < 0.001$, one-way ANOVA.

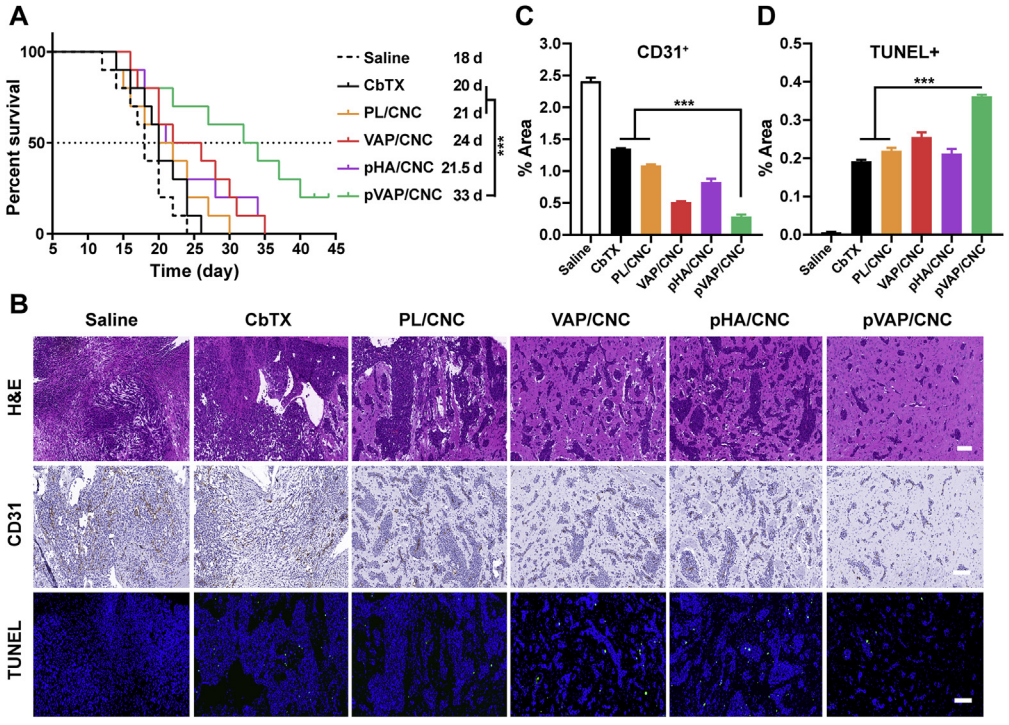

Figure 9 Anti-metastasis activity in 4T1-brain metastatic models. (A) The Kaplan-Meier survival curves of 4T1-brain metastasis-bearing mice treated with saline, CbTX, PL/CNC, VAP/CNC, pHA/CNC or pVAP/CNC at a total CbTX dose of 18 mg/kg ($n = 9$; mean ± SD). (B) The H&E, CD31 and TUNEL staining assay of different therapeutic groups. The area percentage of $CD31^+$ (C) and TUNEL+ (D) in (B) ($n = 3$; mean ± SD). Scale bar = 100 μm ***$P < 0.001$, one-way ANOVA.

TUNEL+ fluorescence intensity in pVAP/CNC group was weaker than that in VAP/CNC group, the pVAP/CNC gained a superiority to the VAP/CNC in the statistical result of % area of TUNEL+ when taking the areas of metastatic lesions into account (Fig. 9B and D). In consideration of the better brain-targeting property of pHA/CNC (Fig. 8) and their poorer performance in anti-brain metastasis in comparison to VAP/CNC (Fig. 9), we speculated that the BBB transporting amounts and the selectivity after crossing BBB were equally important during the brain targeting drug delivery and brain metastasis therapy. In consequence, the outstanding performance of pVAP/CNC in anti-brain metastasis were mainly due to the comprehensive therapeutic advantages based on pHA and VAP.

3.10. Biosafety evaluation

To evaluate the biosafety of pVAP/CNC, the body weight changes were monitored during a drug delivery cycle. The hematological or biochemical analysis were measured after one time drug delivery. The mice treated with pVAP/CNC exhibited a smaller body weight change than that in CbTX group, indicating that pVAP/CNC effectively reduced the systemic side-effect compared with CbTX (Supporting Information Fig. S4A). In addition, the pVAP/CNC did not trigger a significant change in the aspects of hemocyte counts (WBC and PLT) (Fig. S4B and S4C), liver function indexes (Fig. S4D and S4E) and kidney function indexes (Fig. S4F and S4G) as compared with the PBS treatment. From the tissue level, no visible difference was found in the sections of major organs stained with H&E (Fig. S4H) and the brain sections strained with GFAP (Fig. S4I) between the pVAP/CNC and PBS groups, which further demonstrated the low toxicity and biosafety of pVAP/CNC *in vivo*.

4. Conclusions

In summary, we have successfully established a pVAP peptide-decorated platelet membrane-hybrid liposome platform utilizing the advantages of platelet membranes and pVAP peptide. It was confirmed that the incorporated platelet membranes in formulations still retained the specific binding abilities to collagen, fibrinogen as well as tumor cells which were essential for the capture of CTCs *in vivo*. Then, the modification of pVAP peptide were proven significantly enhanced the specific targeting to 4T1 tumor cells, BBB and BTB *in vitro* and *in vivo*. After one cycle of therapy, the pVAP/CNC treatment group eventually achieved a notably improved tumor-inhibitory effects both in orthotopic breast cancer models and corresponding brain metastasis models in comparison to the free CbTX group. Collectively, we provided a multi-targeted drug delivery system with an all-stage targeting property for the whole progression of brain metastatic TNBC, which also might be a safe and promising option for the brain-metastasis from other types of tumors.

Acknowledgments

This work was supported by Shanghai Education Commission Major Project (No. 2017-01-07-00-07-E00052, China), National Natural Science Foundation of China (Nos. 81773657, 81690263, and 81903547, China) and Shanghai Sailing Program (No. 20YF1404500, China).

Author contributions

Weiyue Lu and Zimiao Luo conceived this project. Zimiao Luo designed and carried out the experiments. Sunyi Wu, Jianfen Zhou, Weixia Xu and Qianzhu Xu participated part of the experiments. Linwei Lu, Cao Xie and Yu Liu provided the methodology supporting. Zimiao Luo performed data analysis and wrote the manuscript. All of the authors have read and approved the final manuscript.

Conflicts of interest

All the authors have no conflicts of interest to declare.

Appendix A. Supporting information

Supporting data to this article can be found online at https://doi.org/10.1016/j.apsb.2022.03.026.

References

1. Achrol AS, Rennert RC, Anders C, Soffietti R, Ahluwalia MS, Nayak L, et al. Brain metastases. *Nat Rev Dis Prim* 2019;**5**:5.
2. Foulkes WD, Smith IE, Reis-Filho JS. Triple-negative breast cancer. *N Engl J Med* 2010;**363**:1938−48.
3. Papa A, Caruso D, Tomao S, Rossi L, Zaccarelli E, Tomao F. Triple-negative breast cancer: investigating potential molecular therapeutic target. *Expert Opin Ther Targets* 2015;**19**:55−75.
4. Zhang YJ, Zhu X, Chen XL, Chen QJ, Zhou WX, Guo Q, et al. Activated platelets-targeting micelles with controlled drug release for effective treatment of primary and metastatic triple negative breast cancer. *Adv Funct Mater* 2019;**29**:1806620.
5. Liu Y, Lu WY. Recent advances in brain tumor-targeted nano-drug delivery systems. *Expet Opin Drug Deliv* 2012;**9**:671−86.
6. Monsky WL, Mouta Carreira C, Tsuzuki Y, Gohongi T, Fukumura D, Jain RK. Role of host microenvironment in angiogenesis and microvascular functions in human breast cancer xenografts: mammary fat pad *versus* cranial tumors. *Clin Cancer Res* 2002;**8**:1008−13.
7. Dehaini D, Wei XL, Fang RH, Masson S, Angsantikul P, Luk BT, et al. Erythrocyte-platelet hybrid membrane coating for enhanced nanoparticle functionalization. *Adv Mater* 2017;**29**:1606209.
8. He H, Guo C, Wang J, Korzun WJ, Wang XY, Ghosh S, et al. Leutusome: a biomimetic nanoplatform integrating plasma membrane components of leukocytes and tumor cells for remarkably enhanced solid tumor homing. *Nano Lett* 2018;**18**:6164−74.
9. He YW, Li RX, Li HC, Zhang SY, Dai WT, Wu Q, et al. Erythroliposomes: integrated hybrid nanovesicles composed of erythrocyte membranes and artificial lipid membranes for pore-forming toxin clearance. *ACS Nano* 2019;**13**:4148−59.
10. Ying M, Zhuang J, Wei XL, Zhang XX, Zhang Y, Jiang Y, et al. Remote-loaded platelet vesicles for disease-targeted delivery of therapeutics. *Adv Funct Mater* 2018;**28**:1801032.
11. Bu LL, Rao L, Yu GT, Chen L, Deng WW, Liu JF, et al. Cancer stem cell-platelet hybrid membrane-coated magnetic nanoparticles for enhanced photothermal therapy of head and neck squamous cell carcinoma. *Adv Funct Mater* 2019;**29**:1807733.
12. Rao L, Meng QF, Huang QQ, Wang ZX, Yu GT, Li A, et al. Platelet-leukocyte hybrid membrane-coated immunomagnetic beads for highly efficient and highly specific isolation of circulating tumor cells. *Adv Funct Mater* 2018;**28**:1803531.
13. Gay LJ, Felding-Habermann B. Contribution of platelets to tumour metastasis. *Nat Rev Cancer* 2011;**11**:123−34.
14. Kola SM, Choonara YE, Kumar P, Kondiah PPD, Pillay V. Platelet-inspired therapeutics: current status, limitations, clinical implications, and future potential. *Drug Deliv Transl Res* 2021;**11**:24−48.
15. Ran DN, Mao JN, Shen Q, Xie C, Zhan CY, Wang RF, et al. GRP78 enabled micelle-based glioma targeted drug delivery. *J Control Release* 2017;**255**:120−31.
16. Ran DN, Zhou JF, Chai ZL, Li JY, Xie C, Mao JN, et al. All-stage precisional glioma targeted therapy enabled by a well-designed D-peptide. *Theranostics* 2020;**10**:4073−87.
17. Guo HY, Wang RF, Wang DL, Wang SL, Zhou JF, Chai ZL, et al. Deliver anti-PD-L1 into brain by *p*-hydroxybenzoic acid to enhance immunotherapeutic effect for glioblastoma. *J Control Release* 2020;**320**:63−72.
18. Belhadj Z, Ying M, Cao X, Hu XF, Zhan CY, Wei XL, et al. Design of Y-shaped targeting material for liposome-based multifunctional glioblastoma-targeted drug delivery. *J Control Release* 2017;**255**:132−41.
19. Hu CM, Fang RH, Wang KC, Luk BT, Thamphiwatana S, Dehaini D, et al. Nanoparticle biointerfacing by platelet membrane cloaking. *Nature* 2015;**526**:118−21.
20. Kang T, Zhu QQ, Wei D, Feng JX, Yao JH, Jiang TZ. Nanoparticles coated with neutrophil membranes can effectively treat cancer metastasis. *ACS Nano* 2017;**11**:1397−411.
21. Song YN, Huang ZY, Liu X, Pang ZQ, Chen J, Yang HB. Platelet membrane-coated nanoparticle-mediated targeting delivery of Rapamycin blocks atherosclerotic plaque development and stabilizes plaque in apolipoprotein E-deficient ($ApoE^{-/-}$) mice. *Nanomedicine* 2019;**15**:13−24.
22. Song YN, Huang ZY, Xu JF, Ren DY, Wang Y, Zheng XD, et al. Multimodal SPION-CREKA peptide-based agents for molecular imaging of microthrombus in a rat myocardial ischemia−reperfusion model. *Biomaterials* 2014;**35**:2961−70.
23. Shan W, Zhu X, Liu M, Li L, Zhong JY, Sun W, et al. Overcoming the diffusion barrier of mucus and absorption barrier of epithelium by self-assembled nanoparticles for oral delivery of insulin. *ACS Nano* 2015;**9**:2345−56.
24. Yanes RE, Tarn D, Hwang AA, Ferris DP, Sherman SP, Thomas CR, et al. Involvement of lysosomal exocytosis in the excretion of mesoporous silica nanoparticles and enhancement of the drug delivery effect by exocytosis inhibition. *Small* 2013;**9**:697−704.
25. Fröhlich E. Cellular elimination of nanoparticles. *Environ Toxicol Pharmacol* 2016;**46**:90−4.
26. Luo ZM, Yan ZQ, Jin K, Pang Q, Jiang T, Lu H, et al. Precise glioblastoma targeting by AS1411 aptamer-functionalized poly (L-gamma-glutamylglutamine)-paclitaxel nanoconjugates. *J Colloid Interface Sci* 2017;**490**:783−96.
27. Hu XF, Chai ZL, Lu LW, Ruan HT, Wang RF, Zhan CY, et al. Bortezomib dendrimer prodrug-based nanoparticle system. *Adv Funct Mater* 2019;**29**:1807941.
28. Yang L, Huang L, Liu F. Paclitaxel nanocrystals for overcoming multidrug resistance in cancer. *Mol Pharm* 2010;**7**:863−9.
29. Luo ZM, Jin K, Pang Q, Shen S, Yan ZQ, Jiang T, et al. On-demand drug release from dual-targeting small nanoparticles triggered by high-intensity focused ultrasound enhanced glioblastoma-targeting therapy. *ACS Appl Mater Interfaces* 2017;**9**:31612−25.